Highly Efficient Enrichment of Radionuclides on Graphene Oxide-Supported Polyaniline

ARTICLE *in* ENVIRONMENTAL SCIENCE & TECHNOLOGY · JULY 2013

Impact Factor: 5.33 · DOI: 10.1021/es401174n · Source: PubMed

5 AUTHORS, INCLUDING:

Yubing Sun
Hefei Institute of Physical Sciences, Chinese A…
40 PUBLICATIONS **810** CITATIONS
SEE PROFILE

Changlun Chen
Chinese Academy of Sciences
98 PUBLICATIONS **6,450** CITATIONS
SEE PROFILE

Xiangke Wang
Chinese Academy of Sciences
307 PUBLICATIONS **13,146** CITATIONS
SEE PROFILE

Environmental Science & Technology

Article

pubs.acs.org/est

Highly Efficient Enrichment of Radionuclides on Graphene Oxide-Supported Polyaniline

Yubing Sun, Dadong Shao, Changlun Chen, Shubin Yang, and Xiangke Wang*

Key Laboratory of Novel Thin Film Solar Cells, Institute of Plasma Physics, Chinese Academy of Science, P.O. Box 1126, Hefei, 230031, P. R. China

Supporting Information

ABSTRACT: Graphene oxide-supported polyaniline (PANI@GO) composites were synthesized by chemical oxidation and were characterized by SEM, Raman and FT-IR spectroscopy, TGA, potentiometric titrations, and XPS. The characterization indicated that PANI can be grafted onto the surface of GO nanosheets successfully. The sorption of U(VI), Eu(III), Sr(II), and Cs(I) from aqueous solutions as a function of pH and initial concentration on the PANI@GO composites was investigated. The maximum sorption capacities of U(VI), Eu(III), Sr(II), and Cs(I) on the PANI@GO composites at pH 3.0 and T = 298 K calculated from the Langmuir model were 1.03, 1.65, 1.68, and 1.39 mmol·g^{-1}, respectively. According to the XPS analysis of the PANI@GO composites before and after Eu(III) desorption, nitrogen- and oxygen-containing functional groups on the surface of PANI@GO composites were responsible for radionuclide sorption, and that radionuclides can hardly be extracted from the nitrogen-containing functional groups. Therefore, the chemical affinity of radionuclides for nitrogen-containing functional groups is stronger than that for oxygen-containing functional groups. This paper focused on the application of PANI@GO composites as suitable materials for the preconcentration and removal of lanthanides and actinides from aqueous solutions in environmental pollution management in a wide range of acidic to alkaline conditions.

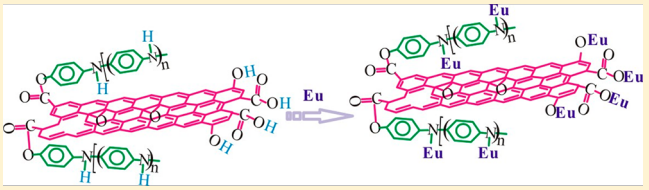

INTRODUCTION

With the peaceful utilization of nuclear energy and the rapid development of nuclear industry, the safe treatment and disposal of high-level wastes in nuclear waste management has always been an environmental concern to the public.[1] Efficient cleanups of these radionuclides by artificial adsorbents such as ion exchange polymers,[2−6] porous media,[7−10] nanoparticles,[11−14] carbon nanotubes,[15−18] and activated carbon (AC)[19−22] have been extensively investigated in recent years. In these studies, the effects of environmental factors (e.g., pH, ionic strength, and humic substances) on radionuclide sorption on artificial adsorbents were investigated extensively. However, the limited sorption capacity hindered their practical application in the removal of radionuclides from large volumes of aqueous solutions.

Graphene oxide (GO) has emerged as a promising material for the removal of heavy metals[23−25] and radionuclides[26−29] in recent years. Zhao et al.[24] found that the maximum sorption capacity of GO for Cd(II) and Co(II) at pH 6.0 and T = 303 K was about 0.95 and 1.16 mmol·g^{-1}, respectively. Romanchuk et al.[29] also demonstrated that GO presented high sorption capacity for radionuclides such as ∼0.76 mmol Eu(III) and 0.12 mmol U(VI) per gram of GO at pH 5.0. However, GO can incur irreversible aggregation and/or polydisperse in its thickness, lateral size, and shape,[30] which may hinder effective sorption behaviors and reduce the sorption capacity. Therefore, a large number of investigators have studied the decoration of GO by introducing various functional groups to enhance its dispersibility and performance.[31−35] Chen et al.[34] reviewed the various functionalization methods for GO such as functionalization with nanoparticles, organic compounds, biomaterials, and polymers. Polyaniline (PANI) is expected to have a strong affinity for heavy metal ions due to large numbers of amine and imine functional groups.[36,37] Poor mechanical solubility and inadequate processability, however, greatly influence its experimental study and commercial application.[38,39] Various PANI composites with excellent sorption capacity have been fabricated to remove heavy metal ions such as Hg(II),[40,41] Cd(II),[42] Cr(VI),[43] Pb(II),[44] etc. To the authors' knowledge, there has been little research on the sorption of radionuclides on GO-supported PANI (PANI@GO composites). Moreover, the interaction mechanism between radionuclides and PANI@GO composites is scarce.

The objectives of the current study were (1) to synthesize PANI@GO composites and to characterize the microscopic and macroscopic surface properties of PANI@GO composites by using SEM, Raman and FT-IR spectroscopy, TGA, potentiometric titrations, and XPS, (2) to investigate the sorption of radionuclides as a function of pH and initial concentration on AC, PANI, GO, and PANI@GO composites by the batch technique, and (3) to discuss the interaction mechanism between radionuclides and PANI@GO composites by using XPS

Received: March 17, 2013
Revised: July 29, 2013
Accepted: July 31, 2013
Published: July 31, 2013

dx.doi.org/10.1021/es401174n | Environ. Sci. Technol. 2013, 47, 9904−9910

Table 1. Selected Parameters for PANI@GO Composites

composition (atom %)[a]	C (69.38%)	N (3.22%)	O (27.37%)
specific surface area (S_{BET}, $m^2 \cdot g^{-1}$)		140.8	
pH_{PZC}[b]		4.6	
concentration of surface active sites ($mol \cdot g^{-1}$)[b]		0.068	

[a]Data from XPS analysis. [b]Data from acid−base titration.

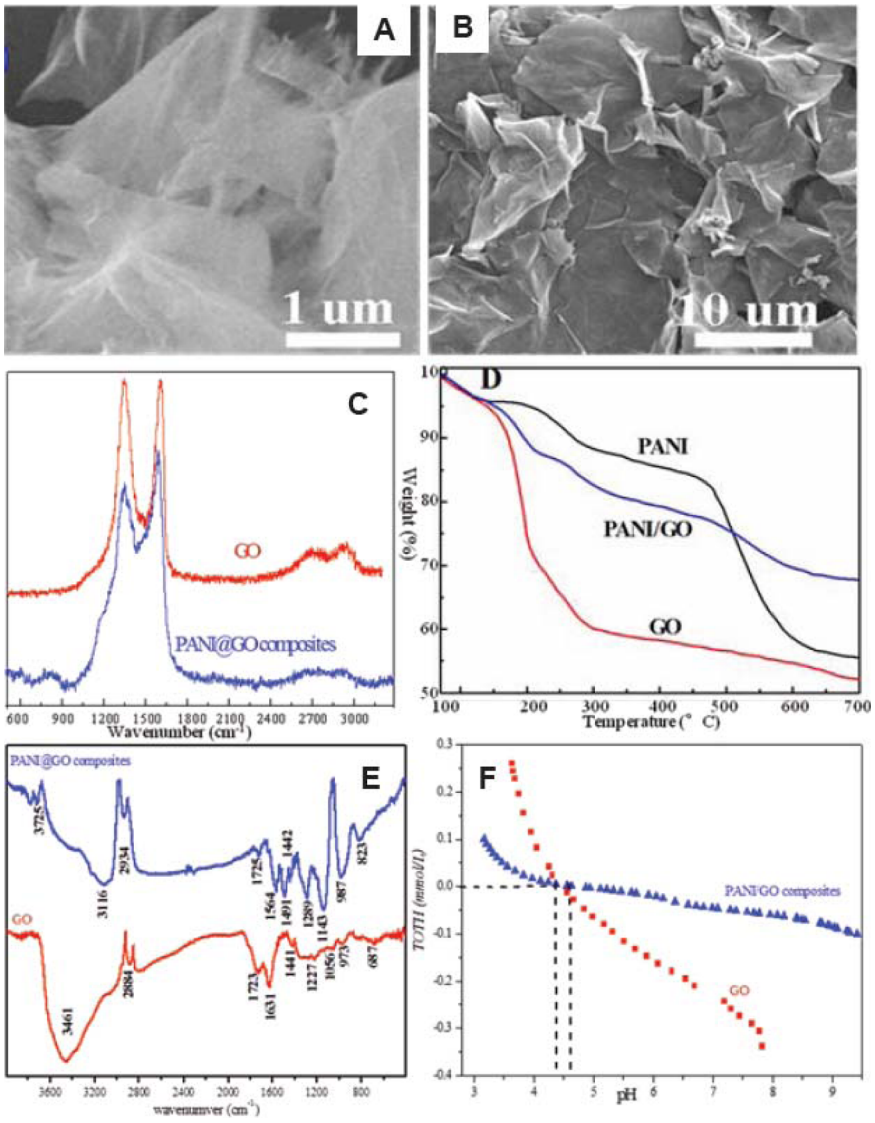

Figure 1. The characterization of PANI@GO composites. A, B: SEM images of GO and PANI@GO composites; C: Raman spectra; D: TGA analysis; E: FT-IR spectra; F: potentiometric acid−base titrations.

spectroscopy. Because of a similar ionic radius and chemical behavior, U(VI) and stable cations (i.e., Eu(III), Sr(II), and Cs(I)) are chosen as chemical analogues of radionuclides in this study. This study highlighted the extensive applicability of this composite in the removal of lanthanides, actinides, and other fission products from large volumes of aqueous solutions in a wide range of acidic to alkaline conditions, which is crucial in the application of these materials in nuclear waste management.

EXPERIMENTAL SECTION

Materials. PANI was synthesized by a chemical oxidation method.[45] Typically, the aniline monomer and ammonium peroxodisulfate ($(NH_4)_2S_2O_8$, AR) were dissolved into HCl solution and stirred vigorously at 60 °C for 3 h under nitrogen-protection conditions. GO nanosheets were obtained from flake graphite (<30 μm, Qingdao, China) by using the modified Hummers method.[46] Briefly, flake graphite and $NaNO_3$ were added into concentrated H_2SO_4 under ultrasonication and ice-bath conditions, $KMnO_4$ was added slowly into the suspension, and the excess MnO_4^- anions were eliminated by adding H_2O_2 (30 wt %) solution. The PANI@GO composites were synthesized by the polymerization of aniline monomer on the amine-terminated GO surface in the presence of $(NH_4)_2S_2O_8$ following the procedure reported by Kumar et al.[47] The specific surface area of PANI@GO composites was 140.8 $m^2 \cdot g^{-1}$ by using the multipoint Brunauer−Emmett−Teller method (Table 1),

dx.doi.org/10.1021/es401174n | Environ. Sci. Technol. 2013, 47, 9904−9910

which is significantly below the theoretical values of 2700 $m^2 \cdot g^{-1}$. This significant difference could be due to collapse of the sheets into relatively large and dense aggregates upon drying.[48] More detailed processes of preparation of PANI, GO, and PANI@GO composites are described in Supporting Information.

U(VI), Eu(III), Sr(II), and Cs(I) stock solutions at 0.1 mol·L^{-1} were prepared from their nitrate (99.9%, Sigma-Aldrich) after dissolution and dilution with 0.01 mol·L^{-1} $HClO_4$ solution. All other reagents (Sinopharm Chemical Reagent Co., Ltd., Shanghai, China) were used directly without further purification in this study.

Characterization of PANI@GO Composites. The PANI@GO composites were characterized by using SEM, Raman spectroscopy, TGA, FT-IR spectroscopy, potentiometric titrations, and XPS. Samples were prepared for SEM by drop-casting a dilute GO suspension on the flat, slightly conductive Si substrate. After gold-coating, the sample was imaged by using a field emission scanning electron microscope (FEI-JSM 6320F). Raman spectroscopy was carried out on the LabRam HR Raman spectrometer at 514.5 nm by an Ar^+ laser. TGA measurements were taken by using a Shimadzu TGA-50 thermogravimetric analyzer from room temperature to 973 K at a heating rate of 10 K·min^{-1} with a nitrogen rate of 50 mL·min^{-1}. The FT-IR spectra of the samples were recorded in pressed KBr pellets (Aldrich, 99%, analytical reagent) by using a Nicolet 8700 FT-IR spectrometer at room temperature. Potentiometric titrations were conducted by using a computer-controlled titration system (DL50 Automatic Titrator, Mettler Toledo). The XPS spectra were recorded on a thermo ESCALAB 250 electron spectrometer with a multidetection analyzer using an Al Kα X-ray source (1486.6 eV) at 10 kV and 5 mA under 10^{-8} Pa residual pressure. The detailed processes of titration and XPS analysis are presented in Supporting Information.

Batch Sorption Measurements. The effect of pH on cation (i.e., 15 mg·L^{-1} of U(VI), Eu(III), Sr(II), and Cs(I)) sorption onto 0.25 g·L^{-1} granular AC (analytical grade, Sinopharm, Shanghai), PANI, GO, and PANI@GO composites was examined at T = 298 K by the batch technique. Their sorption isotherms were investigated at pH 3.0 and T = 298 K within a range of concentrations from 1 to 100 mg·L^{-1}. To eliminate the effect of cation sorption on polycarbonate tube walls, the sorption of cations without adsorbents was carried out under the same experimental conditions. The bulk suspensions of PANI@GO composites and $NaClO_4$ were pre-equilibrated for 24 h, and then cation stock solution was spiked into the bulk suspension gradually. Subsequently, the suspensions were shaken for 48 h to ensure that the sorption reaction could achieve sorption equilibrium (preliminary experiments found that this length of time was adequate for the suspension to obtain equilibrium). The solid and liquid phases were separated by centrifugation at 9000 rpm for 30 min. After centrifugation, the PANI@GO composites containing radionuclides were washed with DI water to remove unabsorbed radionuclides, and then desorption of cations from PANI@GO composites was investigated by using 6 mL of 1.0 mol·L^{-1} HCl (m/V = 0.25 g·L^{-1}) at T = 298 K and under continuous stirring conditions for 6 h. The preliminary desorption kinetics (data not shown) indicated that 6 h was adequate for the suspension to obtain desorption equilibrium by measuring the change in cation concentration in aqueous solution. For all sorption experiments, ^{238}U(VI), ^{154}Eu(III), ^{90}Sr(II), and ^{137}Cs(I) were used to tag the radionuclide nitrate stock solution. The radioactivity of ^{154}Eu(III), ^{90}Sr(II), and ^{137}Cs(I) in suspensions was analyzed by liquid scintillation counting using a Packard 3100 TR/AB liquid scintillation analyzer (Perkin-Elmer) with a scintillation cocktail (ULTIMA GOLD AB, Packard). The radioisotope concentrations of ^{238}U(VI) were analyzed by a kinetic phosphorescence analyzer (KPA-11, Richland, WA). Sorption capacity (Qe, mg·g^{-1}) and removal rate (R, %) for radionuclides by adsorbents at equilibrium were calculated by conducting a mass balance of radionuclides before and after sorption.

RESULTS AND DISCUSSION

Characterization of PANI@GO Composites. As shown in Figure 1A, the SEM image of GO shows that the structure of the GO agglomerates is multilayered with the lateral size ranging from several nanometers to scores of nanometers. A sheetlike morphology of the PANI@GO composites is observed in the SEM images (Figure 1B). According to the Raman spectra of the PANI@GO composites and GO in Figure 1C, the obvious peaks at ~1350 and ~1600 cm^{-1} can be attributed to the disordered structure (D band, sp^3 carbon atoms of defects and disorders) and graphite structure (G band, sp^2 carbon atoms in graphitic sheets) of GO, respectively. Compared to GO, the position of the D band of the PANI@GO composites (~1340 cm^{-1}) is gradually shifted to lower frequencies, which can be due to the fact that the electron pairs of the N atoms of PANI resonate with the adjacent benzene structures of GO.[49,50] A three-step weight loss of the GO and PANI@GO composites is observed as indicated by the TGA curves (Figure 1D). The weight loss in the first step up to ~120 °C can be due to the loss of moisture, and the other two steps of mass loss are observed up to ~210 °C and up to ~320 °C, which are related to the loss of CO and CO_2 from the decomposition of carbon-oxidized and oxygen-containing functional groups, respectively.[51] PANI shows a two-step weight loss from 200 °C to 600 °C due to the elimination of the doped acid bound to PANI chains and the decomposition of the pristine PANI backbone, respectively. For PANI@GO composites, the lower rate of mass loss with increasing temperature could be due to the internal change in this material that is not accompanied by mass loss at elevated temperature. As illustrated in Figure 1E, the FT-IR spectrum of the GO nanosheets shows characteristic bands at 687 cm^{-1} (C−H out-of-plane on the 1,2-ring),[47] at 973 cm^{-1} (C−H in-plane on the 1,2,4-ring),[47] at 1056 and 1227 cm^{-1} (C−O bond),[27] at 1441 cm^{-1} (stretching of benzene ring),[47] at 1631 cm^{-1} (sp^2 C═C bond),[27] at 1723 cm^{-1} (C═O stretching vibration),[47] and at 3461 cm^{-1} (OH stretching vibration).[27] Compared to GO nanosheets, the FT-IR spectrum of the PANI@GO composites presents similar characteristic peaks related to the C−H out-of-plane (~823 cm^{-1}), C−H in-plane (987 cm^{-1}), and C═O stretching vibration (1723 cm^{-1}). Interestingly, the characteristic bands at 1143, 1491, and 1564 cm^{-1} are attributed to the N−Q−N−Q stretch of the quinonoid (Q) ring, benzenoid ring vibration (C═C stretching deformations), and quinonoid ring vibration (N═Q═N),[47,52] respectively. It is determined that the band at ~3116 cm^{-1} is attributable to the ═N−H stretching model.[53] The shift of the band at 1725 cm^{-1} is associated with the stretching mode of the ester linkages between the acyl-functionalized GO and the aminophenol derivative, suggesting a covalent linkage.[47] The characteristic band attributed to the N−Q−N−Q stretching of the quinonoid ring indicates that PANI has been covalently grafted onto the surface of GO, which is consistent with the work by Kumar et al.[47] The other bands (e.g., 2934 cm^{-1} for PANI@GO composites, and 2884 cm^{-1} for GO) are attributed to impurity or sum frequencies.[51] According to potentiometric

acid−base titrations (Figure 1F), the rate of TOTH change for PANI@GO composites is significantly lower than that for GO, which could be due to the large number of nitrogen- and oxygen-containing functional groups. The pH_{PZC} (point of zero charge) of GO and PANI@GO composites are ~4.4 and ~4.6, respectively. The subtle change in pH_{PZC} between GO and PANI@GO composites could be due to the lower value of the pK_a of PANI from the protonated amine (NH_2^+, 2.5) and protonated imine (=NH^+, 5.5).[54] For PANI@GO composites, the concentration of surface-active sites is calculated to be 0.068 mol·g^{-1} in terms of acidic titration (Table 1). The concentration of surface-active sites is much higher than that for GO (~0.0036 mol·g^{-1}),[27] which is due to the introduction of massive nitrogen-containing functional groups on the surface of the PANI@GO composites. More details on the calculation of the concentration of surface-active sites are reported in our previous work.[27]

Effect of pH. The effect of pH on U(VI), Eu(III), Sr(II), and Cs(I) sorption onto AC, PANI, GO, and PANI@GO composites are investigated by the batch technique in the presence of 0.01 mol·L^{-1} $NaClO_4$ solution (Figure 2). As illustrated in Figure 2,

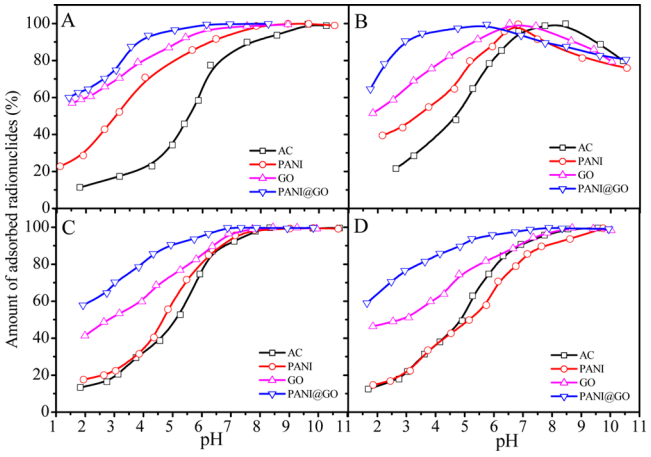

Figure 2. The pH-dependent sorption of radionuclides on AC, PANI, GO, and PANI@GO composites. A: Eu(III); B: U(VI); C: Sr(II); D: Cs(I), $C_{initial}$ = 15 mg·L^{-1}, m/V = 0.25 g·L^{-1}, I = 0.01 mol·L^{-1} $NaClO_4$, T = 298 K.

the sorption of cations on AC, PANI, GO, and PANI@GO composites increases significantly with increasing pH ranging from 2.0 to 7.0, which can be attributed to electrostatic attraction between the negative charge of adsorbents and the positive charge of cations. The reduced sorption of U(VI) on PANI@GO composites at pH > 7.0 could be attributed to the formation of negatively charged species of uranium with carbonate from the atmosphere (Table S1 and Figure S1 in Supporting Information). The electrostatic repulsion between $(UO_2)_3(OH)_7^-$ or $UO_2(CO_3)_2^{2-}$ species and PANI@GO composites with negative charge (pH > pH_{PZC}) would inhibit the sorption of uranium ions on the PANI@GO composites. The other cations' (i.e., Eu(III), Sr(II), and Cs(I)) sorption onto the PANI@GO composites maintain a high level at pH > 7.0 due to precipitation/coprecipitation. Compared to granular AC, PANI, and GO, enhanced sorption of radionuclides on the PANI@GO composites is due to the occurrence of a large number of nitrogen- and oxygen-containing functional groups, which form strong complexes with cations.

Sorption Isotherms. A higher sorption of cations on the PANI@GO composites is observed at high pH values (Figure 2), whereas the solution pH values of nuclear wastewater are generally low. Therefore, it is important to evaluate the sorption capacity of the PANI@GO composites at low pH values. As illustrated in Figure 3, the sorption capacity of the PANI@GO

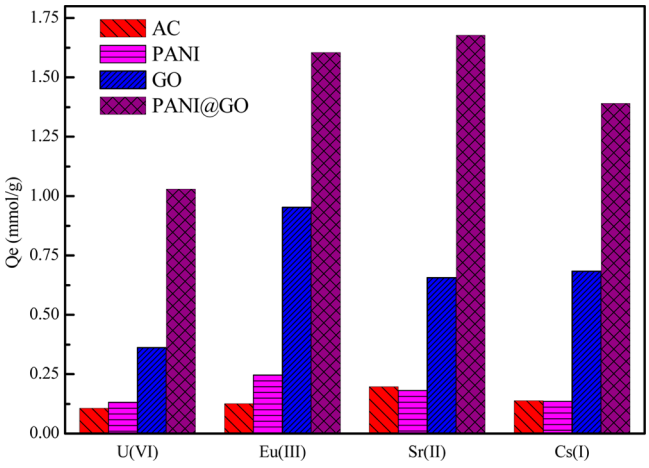

Figure 3. Comparison of the sorption capacity of PANI@GO composites with other adsorbents for the uptake of radionuclides, pH = 3.0, T = 298 K, m/V = 0.25 g·L^{-1}.

composites for cations is significantly higher than that of AC at pH 3.0. The sorption of cations on AC, PANI, GO, and PANI@GO composites is fitted by using Langmuir and Freundlich models (Table S2 in Supporting Information). As shown in Table S2, the sorption of cations on the PANI@GO composites can be fitted by the Langmuir model very well (R^2 > 0.99). The maximum sorption capacities of the PANI@GO composites calculated for the Langmuir model at pH 3.0 and T = 298 K are 1.03 and 1.65 mmol·g^{-1} for U(VI) and Eu(III), respectively, which is approximately 1 order of magnitude higher than that of AC (0.11 and 0.13 mmol·g^{-1} for U(VI) and Eu(III), respectively). From an investigation of the literature (Table S3 in Supporting Information), the PANI@GO composites yield a more remarkable enhancement for cations at acidic conditions. Combined with sorption behaviors of cations at high pH, there is no doubt that the PANI@GO composites could be used as a suitable material for the preconcentration and removal of radionuclides from aqueous solutions over a wide range of pH in environmental pollution cleanup.

Sorption Mechanism. To determine the interaction mechanism between radionuclides and PANI@GO composites, the XPS spectra of survey and high resolution scans for O 1s, N 1s, and Eu 3d on the PANI@GO composites before and after Eu(III) desorption (denoted as PANI@GO-Eu and PANI@GO-Eu-HCl, respectively) were recorded as shown in Figure 4. In the survey spectra in Figure 4A, the occurrence of Eu 3d of PANI@GO-Eu is in accord with a shift in binding energy and a decrease in peak area of N 1s and O 1s spectra (Table 2). For the PANI@GO-Eu-HCl sample, an apparent increase in the peak area of N 1s and O 1s and a corresponding decrease in the peak area of Eu 3d are observed. The desorption of Eu(III) freed nitrogen and oxygen and led to an increase in the N 1s and O 1s peaks. Wang et al.[36] also found an apparent decrease in Hg 4f peak area and a corresponding increase in N 1s peak area for PANI-Hg with 1 mol/L HCl. The authors suggested that sorption of Hg(II) on PANI mainly involved nitrogen, so the desorption of Hg(II) freed nitrogen and led to an increase in the N 1s peak. The survey scans of XPS spectra clearly demostrate that the sorption of

dx.doi.org/10.1021/es401174n | Environ. Sci. Technol. 2013, 47, 9904−9910

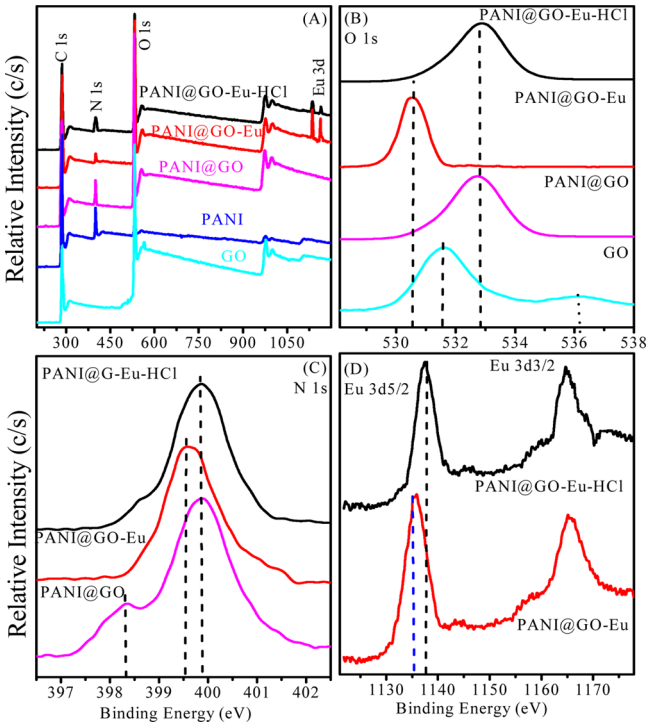

Figure 4. XPS survey scan and high resolution scans of GO, PANI, PANI@GO, PANI@GO-Eu, and PANI@GO-Eu-HCl. (A) Total survey scans; (B) O 1s peaks; (C) N 1s peaks; (D) Eu 3d peaks, m/V = 0.25 g·L^{-1}, pH = 3.0, I = 0.01 mol·L^{-1} $NaClO_4$.

Table 2. Binding Energies of GO, PANI, and PANI@GO Composites before and after Desorption

adsorbents	O 1s (eV)	N 1s (eV)	Eu 3d5/2 (eV)	Eu 3d3/2 (eV)
GO	531.57			
PANI	531.95	399.85		
PANI@GO	532.73	399.65		
PANI@GO-Eu	530.56	399.16	1134.9	1164.3
PANI@GO-Eu-HCl	532.86	400.18	1137.4	1164.7

europium on PANI@GO composites is relevant to both nitrogen and oxygen functional groups.

As illustrated in Table 2, the binding energy of O 1s of PANI@GO-Eu (530.56 eV) is lower than that of PANI@GO-Eu-HCl (532.86 eV), which is due to the increase of negative charge of the oxygen atom in the coordinated PANI@GO composites after desorption.[55] The peak fitting of the O 1s of GO, PANI, PANI@GO-Eu, and PANI@GO-Eu-HCl is shown in Figure S3A in Supporting Information. For the GO sample, three major O 1s peaks positioned at 531.28 eV (bridging OH), 532.28 eV (terminal OH), and 536.18 eV (adsorbed H_2O) are observed.[56] However, the relative intensity of the peak for adsorbed H_2O disappears while an increase in the relative intensity of the terminal OH peak of PANI, PANI@GO-Eu, and PANI@GO-Eu-HCl is observed. The results of XPS spectral analysis indicate that the higher sorption capacity of the PANI@GO composites can be greatly attributed to the occurrence of a large number of oxygen-containing functional groups, which can bind to cations easily.

A higher binding energy of N 1s of PANI@GO-Eu-HCl (at 400.18 eV) is also observed compared to that of PANI@GO-Eu (at 399.16 eV), which is consistent with the change in binding energy of O 1s (Table S2). The change in binding energy of N 1s (~ 1.0 eV) is lower than that of O 1s (2.3 eV) between PANI@GO-Eu-HCl and PANI@GO-Eu samples, indicating that the nitrogen-containing functional groups present the main contribution to irreversible sorption of Eu(III) to PANI@GO composites. As shown in Figure S3C in Supporting Information, the high resolution scans for N 1s in the PANI@GO composites could be grouped into three peaks at ~398.28, ~399.78, and ~400.38 eV, corresponding to imine (N═), amine (NH), and protonated amine (NH_2^+), respectively, which is consistent with the results reported by Kang et al.[53] In the case of the PANI@GO-Eu and PANI@GO-Eu-HCl systems, the relative intensity of the amine (NH) group for PANI@GO-Eu-HCl significantly decreases, whereas the relative intensity and position of the protonated amine (NH_2^+) group display a subtle change between PNAI@GO-Eu and PANI@GO-Eu-HCl samples, indicating that europium mainly bonds to protonated amine groups. Therefore, it is plausible that protonated amine groups present the main contribution to the irreversible sorption of Eu(III) to PANI@GO composites.

Eu 3d spectra of PANI@GO-Eu and PANI@GO-Eu-HCl could be characterized with two doublet peaks, including Eu $3d_{5/2}$ (at ~1134/1137 eV) and Eu $3d_{3/2}$ (at 1165 eV) peaks (Figure 4D). Compared to PANI@GO-Eu, the position of Eu $3d_{5/2}$ of PANI@GO-Eu-Cl is shifted to higher binding energy while its relative intensity is decreased. Combined with the difference in binding energy and relative intensity of O 1s of PANI@GO-Eu and PANI@GO-Eu-HCl, it is demonstrated that radionuclides can be extracted from oxygen-containing functional groups much more easily compared to that from nitrogen-containing functional groups. As shown in Figure S3D, the occurrence of two Eu 3d5/2 fitting peaks in the high resolution XPS scans shows that europium could be complexed with two types of binding sites on the PANI@GO composites (denoted Eu_1 and Eu_2 binding sites). Wang et al.[36] also found that the existence of two Hg4f doublets (Hg_1 and Hg_2) in the high resolution XPS spectra of PANI containing mercury, indicating that mercury could be complexed to two types of general binding sites. According to the calculation of area of the Eu 3d5/2 peak, approximately 34.5% and 0.3% of europium is desorbed from Eu_1 and Eu_2 sites of the Eu $3d_{5/2}$ peak, respectively, indicating qualitatively that it is not easier to extract Eu(III) cation from Eu_2 sites compared that from Eu_1 sites. Combined with the change in O 1s and N 1s of PANI@GO-Eu and PANI@GO-Eu-HCl composites, the binding energy of Eu $3d_{5/2}$ and O 1s of PANI@GO-Eu is lower by ~2.0 eV compared to that of PANI@GO-Eu-HCl, while the change in binding energy of N 1s for PANI@GO-Eu and PANI@GO-Eu-HCl composites is lower than that of O 1s. Therefore, the results of XPS spectral analysis indicate that the sorption of radionuclides by nitrogen- and oxygen-containing functional groups (e.g., imine, amine, protonated amine, hydroxyl, and carboxyl group) of PANI@GO composites is observed, and that radionuclides can hardly be extracted from nitrogen-containing functional groups. Therefore, the chemical affinity of radionuclides for nitrogen-containing functional groups is stronger than that for oxygen-containing functional groups.

In conclusion, it has been demonstrated that PANI can be grafted onto the surface of GO nanosheets by using a chemical method. The PANI@GO composites demonstrate versatile and highly efficient enrichment of radionuclides at a wide range of acidic to alkaline conditions. The sorption of radionuclides on PANI@GO composites occurs by the formation of complexes

dx.doi.org/10.1021/es401174n | Environ. Sci. Technol. 2013, 47, 9904−9910

with the nitrogen- and oxygen-containing functional groups, and the chemical affinity of the radionuclides for the nitrogen-containing functional groups is stronger than that for the oxygen-containing functional groups. These GO-based materials represent potentially suitable materials for the preconcentration and removal of radionuclides in environmental pollution cleanup and nuclear waste management, especially at low pH values.

■ ASSOCIATED CONTENT

Supporting Information

The preparation of PANI@GO composites and the calculation of the maximum sorption capacity of radionuclides. This material is available free of charge via the Internet at http://pubs.acs.org.

■ AUTHOR INFORMATION

Corresponding Author

*Phone: +86-551-65592788; fax: +86-551-65591310; e-mail: xkwang@ipp.ac.cn (X.W.).

Notes

The authors declare no competing financial interest.

■ ACKNOWLEDGMENTS

Financial support from 973 projects from Ministry of Science and Technology of China (2011CB933700), National Natural Science Foundation of China (21207135, 21007074, 21207136, 21225730, and 91126020), and Hefei Center for Physical Science and Technology (2012FXZY005) is acknowledged.

■ REFERENCES

(1) Coughtrey, P. J.; Thorne, M. C. *Radionuclide distribution and transport in terrestrial and aquatic ecosystems. A critical review of data*; Balkema: Rotterdam, Netherlands, 1983; Vol. *1*.

(2) Jain, V. K.; Handa, A.; Sait, S. S.; Shrivastav, P.; Agrawal, Y. K. Preconcentration, separation and trace determination of lanthanum (III), cerium (III), and uranium (VI) on polymer supported σ-vanillinsemicarbazone. *Anal. Chim. Acta* **2001**, *429*, 237−246.

(3) Monsallier, J. M.; Schussler, W.; Buckau, G.; Rabung, T.; Kim, J. Kinetic investigation of Eu(III)−humate interactions by ion exchange resins. *Anal. Chem.* **2003**, *75*, 3168−3174.

(4) Gu, B.; Ku, Y. K.; Jardine, P. M. Sorption and binary exchange of nitrate, sulfate, and uranium on an anion-exchange resin. *Environ. Sci. Technol.* **2004**, *38*, 3184−3188.

(5) Wang, X. K.; Chen, C. L.; Du, J. Z.; Tan, X. L.; Xu, D.; Yu, S. M. Effect of pH and aging time on the kinetic dissociation of ^{243}Am(III) from humic acid-coated γ-Al_2O_3: A chelating resin exchange study. *Environ. Sci. Technol.* **2005**, *39*, 7084−7088.

(6) Wang, X. K.; Zhou, X.; Du, J. Z.; Hu, W. P.; Chen, C. L.; Chen, Y. X. Using of chelating resin to study the kinetic desorption of Eu(III) from humic acid−Al_2O_3 colloid surfaces. *Surf. Sci.* **2006**, *600*, 478−483.

(7) Warwick, P. W.; Hall, A.; Pashley, V.; Bryan, N. D.; Griffin, D. Modelling the effect of humic substances on the transport of europium through porous media: A comparison of equilibrium and equilibrium/kinetic models. *J. Contam. Hydrol.* **2000**, *42*, 19−34.

(8) Um, W.; Mattigod, S.; Serne, R. J.; Fryxell, G. E.; Kim, D. H.; Troyer, L. D. Synthesis of nanoporous zirconium oxophosphate and application for removal of U(VI). *Water Res.* **2007**, *41*, 3217−3226.

(9) Sun, Y. B.; Yang, S. T.; Sheng, G. D.; Guo, Z. Q.; Tan, X. L.; Xu, J. Z.; Wang, X. K. Comparison of U(VI) removal from contaminated groundwater by nanoporous alumina and non-nanoporous alumina. *Sep. Purif. Technol.* **2011**, *83*, 196−203.

(10) Kasap, S.; Piskin, S.; Tel, H. Titanate nanotubes: preparation, characterization and application in adsorption of strontium ion from aqueous solution. *Radiochim. Acta* **2012**, *100*, 925−929.

(11) Tan, X. L.; Wang, X. K.; Fang, M.; Chen, C. L. Sorption and desorption of Th(IV) on nanoparticles of anatase studied by batch and spectroscopy methods. *Colloids Surf., A* **2007**, *296*, 109−116.

(12) Zeng, H.; Singh, A.; Basak, S.; Ulrich, K. U.; Sahu, M.; Biswas, P.; Catalano, J. G.; Giammar, D. E. Nanoscale size effects on uranium(VI) adsorption to hematite. *Environ. Sci. Technol.* **2009**, *43*, 1373−1378.

(13) Yan, S.; Hua, B.; Bao, Z. Y.; Yang, J.; Liu, C. X.; Deng, B. L. Uranium(VI) removal by nanoscale zerovalent iron in anoxic batch systems. *Environ. Sci. Technol.* **2010**, *44*, 7783−7789.

(14) Sun, Y. B.; Yang, S. T.; Sheng, G. D.; Wang, Q.; Guo, Z. Q.; Wang, X. K. Removal of U(VI) from aqueous solutions by the nano-iron oxyhydroxides. *Radiochim. Acta* **2012**, *100*, 779−784.

(15) Wang, X. K.; Chen, C. L.; Hu, W. P.; Ding, A. P.; Xu, D.; Zhou, X. Sorption of ^{243}Am(III) to multiwall carbon nanotubes. *Environ. Sci. Technol.* **2005**, *39*, 2856−2860.

(16) Chen, C. L.; Li, X. L.; Wang, X. K. Application of oxidized multiwall carbon nanotubes for Th(IV) adsorption. *Radiochim. Acta* **2007**, *95*, 261−266.

(17) Chen, C. L.; Wang, X. K.; Nagatsu, M. Europium adsorption on multiwall carbon nanotube/iron oxide magnetic composite in the presence of polyacrylic acid. *Environ. Sci. Technol.* **2009**, *43*, 2362−2367.

(18) Shao, D. D.; Jiang, Z. Q.; Wang, X. K.; Li, J. X.; Meng, Y. D. Plasma-induced grafting carboxymethyl cellulose on multiwalled carbon nanotubes for the removal of UO_2^{2+} from aqueous solution. *J. Phys. Chem. B* **2009**, *113*, 860−864.

(19) Mellah, A.; Chegrouche, S.; Barkat, M. The removal of uranium (VI) from aqueous solutions onto activated carbon: Kinetic and thermodynamic investigations. *J. Colloid Interface Sci.* **2006**, *296*, 434−441.

(20) Gad, H. M. H.; Awwad, N. S. Factors affecting on the sorption/desorption of Eu(III) using activated carbon. *Sep. Sci. Technol.* **2007**, *42*, 3657−3680.

(21) Shawabkeh, R. A.; Rockstraw, D. A.; Bhada, R. K. Copper and strontium adsorption by a novel carbon material manufactured from pecan shells. *Carbon* **2002**, *40*, 781−786.

(22) Song, K. C.; Lee, H. K.; Moon, H.; Lee, K. J. Simultaneous removal of the radiotoxic nuclides Cs^{137} and I^{129} from aqueous solution. *Sep. Purif. Technol.* **1997**, *12*, 215−227.

(23) Yang, S. T.; Chang, Y. L.; Wang, H. F.; Liu, G. B.; Chen, S.; Wang, Y. W.; Liu, Y. F.; Cao, A. N. Folding/aggregation of graphene oxide and its application in Cu^{2+} removal. *J. Colloid Interface Sci.* **2010**, *351*, 122−127.

(24) Zhao, G. X.; Li, J. X.; Ren, X. M.; Chen, C. L.; Wang, X. K. Few-layered graphene oxide nanosheets as superior sorbents for heavy metal ion pollution management. *Environ. Sci. Technol.* **2011**, *45*, 10454−10462.

(25) Sitko, R.; Turek, E.; Zawisza, B.; Malicka, E.; Talik, E.; Heimann, J.; Gagor, A.; Feist, B.; Wrzalik, R. Adsorption of divalent metal ions from aqueous solutions using graphene oxide. *Dalton Trans.* **2013**, *42*, 5682−5689.

(26) Zhao, G. X.; Wen, T.; Yang, X.; Yang, S. B.; Liao, J. L.; Hu, J.; Shao, D. D.; Wang, X. K. Preconcentration of U(VI) ions on few-layered graphene oxide nanosheets from aqueous solutions. *Dalton Trans.* **2012**, *41*, 6182−6188.

(27) Sun, Y. B.; Wang, Q.; Chen, C. L.; Tan, X. L.; Wang, X. K. Interaction between Eu(III) and graphene oxide nanosheets investigated by batch and extended X-ray absorption fine structure spectroscopy and by modeling techniques. *Environ. Sci. Technol.* **2012**, *46*, 6020−6027.

(28) Li, Z.; Chen, F.; Yuan, L.; Liu, Y.; Zhao, Y.; Chai, Z.; Shi, W. Uranium(VI) adsorption on graphene oxide nanosheets from aqueous solutions. *Chem. Eng. J.* **2012**, *210*, 539−946.

(29) Romanchuk, A. Y.; Slesarev, A. S.; Kalmykov, S. N.; Kosynkin, D. V.; Tour, J. M. Graphene oxide for effective radionuclide removal. *Phys. Chem. Chem. Phys.* **2013**, *12*, 2321−2327.

(30) Green, A. A.; Hersam, M. C. Emerging methods for producing monodisperse graphene dispersions. *J. Phys. Chem. Lett.* **2010**, *1*, 544−549.

(31) Goncalves, G.; Marques, P. A.; Barros-Timmons, A.; Bdkin, I.; Singh, M. K.; Emami, N.; Gracio, J. Graphene oxide modified with PMMA via ATRP as a reinforcement filler. *J. Mater. Chem.* **2010**, *20*, 9927−9934.
(32) Pham, T. A.; Kumar, N. A.; Jeong, Y. T. Covalent functionalization of graphene oxide with polyglycerol and their use as templates for anchoring magnetic nanoparticles. *Synth. Met.* **2010**, *160*, 2028−2036.
(33) Li, G. L.; Liu, G.; Li, M.; Wan, D.; Neoh, K. G.; Kang, E. T. Organo- and water-dispersible graphene oxide-polymer nanosheets for organic electronic memory and gold nanocomposites. *J. Phys. Chem. C* **2010**, *114*, 12742−12748.
(34) Li, Y.; Gao, W.; Ci, L.; Wang, C.; Ajayan, P. M. Catalytic performance of Pt nanoparticles on reduced graphene oxide for methanol electro-oxidation. *Carbon* **2010**, *48*, 1124−1130.
(35) Chen, D.; Feng, H. B.; Li, J. H. Graphene oxide: preparation, functionalization, and electrochemical applications. *Chem. Rev.* **2012**, *112*, 6027−6053.
(36) Wang, J.; Deng, B.; Chen, H.; Wang, X.; Zheng, J. Removal of aqueous Hg(II) by polyaniline: Sorption characteristics and mechanisms. *Environ. Sci. Technol.* **2009**, *43*, 5223−5228.
(37) Yang, L.; Wu, S.; Chen, J. P. Modification of activated carbon by polyaniline for enhanced adsorption of aqueous arsenate. *Ind. Eng. Chem. Res.* **2007**, *46*, 2133−2140.
(38) Bhadra, S.; Singha, N. K.; Khastgir, D. Effect of aromatic substitution in aniline on the properties of polyaniline. *Eur. Polym. J.* **2008**, *44*, 1763−1770.
(39) Wang, Z.; Liu, E.; Gu, D.; Wang, Y. Glassy carbon electrode coated with polyaniline-functionalized carbon nanotubes for detection of trace lead in acetate solution. *Thin Solid Films* **2011**, *519*, 5280−5284.
(40) Gupta, R. K.; Singh, R. A.; Dubey, S. S. Removal of mercury ions from aqueous solutions by composite of polyaniline with polystyrene. *Sep. Purif. Technol.* **2004**, *38*, 225−232.
(41) Zhang, Y.; Li, Q.; Sun, L.; Tang, R.; Zhai, J. High efficient removal of mercury from aqueous solution by polyaniline/humic acid nanocomposite. *J. Hazard. Mater.* **2010**, *175*, 404−409.
(42) Mansour, M. S.; Ossman, M. E.; Farag, H. A. Removal of Cd(II) ion from waste water by adsorption onto polyaniline coated on sawdust. *Desalination* **2011**, *272*, 301−305.
(43) Bhaumik, M.; Maity, A.; Srinivasu, V. V.; Onyango, M. S. Removal of hexavalent chromium from aqueous solution using polypyrrole-polyaniline nanofibers. *Chem. Eng. J.* **2012**, *181−182*, 323−333.
(44) Shao, D. D; Chen, C. L.; Wang, X. K. Application of polyaniline and multiwalled carbon nanotube magnetic composites for removal of Pb(II). *Chem. Eng. J.* **2012**, *185−186*, 144−150.
(45) Shimano, J. Y.; MacDiarmid, A. G. Polyaniline, a dynamic block copolymer: Key to attaining its intrinsic conductivity? *Synth. Met.* **2001**, *123*, 251−262.
(46) Hummers, W. S.; Offeman, R. E. Preparation of graphitic oxide. *J. Am. Chem. Soc.* **1958**, *80*, 1339−1339.
(47) Kumar, N. A.; Choi, H. J.; Shin, Y. R.; Chang, D. W.; Dai, L.; Baek, J. B. Polyaniline-grafted reduced graphene oxide for efficient electrochemical supercapacitors. *ACS Nano* **2012**, *6*, 1715−1723.
(48) Whitby, R. L. D.; Guńko, V. M.; Korobeinyk, A.; Busquets, R.; Cundy, A. B.; Laszlo, K.; Skubiszewska-Zieba, J.; Leboda, R.; Tombacz, E.; Toth, I. Y.; Kovacs, K.; Mikhalovsky, S. V. Driving forces of conformational changes in single-layer graphene oxide. *ACS Nano* **2012**, *6*, 3967−3973.
(49) Rao, P. S.; Sathyanarayana, D. N.; Palaniappan, S. Polymerization of aniline in an organic peroxide system by the inverted emulsion process. *Macromolecules* **2002**, *35*, 4988−4996.
(50) Hsiao, M. C.; Liao, S. H.; Yen, M. Y.; Liu, P. I.; Pu, N. W.; Wang, C. A.; Ma, C. C. M. Preparation of covalently functionalized graphene using residual oxygen-containing functional groups. *ACS Appl. Mater. Interfaces* **2010**, *2*, 3092−3099.
(51) Liu, P.; Liu, W.; Xue, Q. In situ chemical oxidative graft polymerization of aniline from silica nanoparticles. *Mater. Chem. Phys.* **2004**, *87*, 109−113.
(52) Tang, J. S.; Jing, X. B.; Wang, B. C.; Wang, F. S. Infrared spectra of soluble polyaniline. *Synth. Met.* **1988**, *24*, 231−238.
(53) Kang, E. T.; Neoh, K. G.; Tan, K. L. Polyaniline: A polymer with many interesting intrinsic redox states. *Prog. Polym. Sci.* **1998**, *23*, 277−324.
(54) Menardo, C.; Nechtschein, M.; Rousseau, A.; Travers, J. P. Investigating on the structure of polyaniline: ^{13}C n.m.r. and titration studies. *Synth. Met.* **1988**, *25*, 311−322.
(55) Wang, L. H.; Wang, W.; Zhang, W. G.; Kang, E. T.; Huang, W. Synthesis and luminescence properties of novel Eu-containing copolymers consisting of Eu(III)−acrylate−β-diketonate complex monomers and methyl methacrylate. *Chem. Mater.* **2000**, *12*, 2212−2218.
(56) Tan, X. L.; Fan, Q. H.; Wang, X. K.; Grambow, B. Eu(III) sorption to TiO_2 (anatase and rutile): Batch, XPS, and EXAFS studies. *Environ. Sci. Technol.* **2009**, *43*, 3115−3121.